Earth Movers Distance-Based Simultaneous Comparison of Hyperspectral Endmembers and Proportions

Alina Zare, *Member, IEEE*, and Derek T. Anderson, *Member, IEEE*

***Abstract*—A new approach for simultaneously comparing sets of hyperspectral endmembers and proportion values using the Earth Movers Distance (EMD) is presented. First, the EMD is defined and calculated per-pixel based on the proportion values and corresponding endmembers. Next, these per-pixel EMD distances are aggregated to obtain a final measure of dissimilarity. In particular, the proposed EMD approach can be used to simultaneously compare endmembers and proportion values with differing numbers of endmembers. The proposed method has a number of uses, including: computing the similarity between two sets of endmembers and proportion values that were obtained using any algorithm or underlying mixing model, clustering sets of hyperspectral endmember and proportion values, or evaluating spectral unmixing results by comparing estimated values to ground truth information. Experiments on both simulated and measured hyperspectral data sets demonstrate that the EMD is effective at simultaneous endmember and proportion comparison.**

I. Introduction

HYPERSPECTRAL imagery contains the radiance or reflectance values across hundreds of narrow, contiguous wavelengths for a given spatial region. Collection and analysis of hyperspectral imagery has been conducted for a wide variety of applications including plant and soil mapping [1]–[3], urban remote sensing [4], [5], planetary applications [6], [7], and others. A significant motivation for the use of hyperspectral imagery is the potential to conduct sub-pixel analysis. A prominent approach for sub-pixel analysis of hyperspectral imagery is through the application of spectral unmixing and endmember estimation methods. In these approaches, the spectral signatures of the pure, constituent materials of a scene, termed *endmembers*, and the sub-pixel amounts of each of these materials in every spatial location, termed *proportion values*, are estimated given an assumed mixing model. Mixing models for hyperspectral imagery include the linear mixing model in which pixels are modeled as convex combinations of endmember spectra as well as a number of non-linear mixing models.

Manuscript received May 02, 2013; revised May 29, 2013, August 02, 2013; accepted August 22, 2013. Date of publication September 16, 2013; date of current version August 01, 2014.

A. Zare is with the Department of Electrical and Computer Engineering, University of Missouri, Columbia, MO 65211 USA (e-mail: zarea@missouri.edu).

D. T. Anderson is with the Electrical and Computer Engineering Department, Mississippi State University, Mississippi State, MS 39762 USA (e-mail: anderson@ece.msstate.edu).

Color versions of one or more of the figures in this paper are available online at http://ieeexplore.ieee.org.

Digital Object Identifier 10.1109/JSTARS.2013.2279753

Regardless of the assumed mixing model, spectral unmixing method, or endmember estimation algorithm employed, a number of approaches have been developed in the literature to compare endmember spectral signatures and to compare proportion values. Methods to compare endmembers have been used to evaluate endmember estimation algorithms when ground truth spectra are available [9], [10], compare endmembers during endmember estimation [11], and other applications. Methods to compare proportion values have generally been conducted for evaluation of spectral unmixing results when ground truth information (such as with simulated data) is available. Previous methods only compare either pairs of endmembers or proportions separately. These previous methods have the following primary limitations:

1) Previous endmember comparison methods can only compare two endmembers at a time.
2) Previous proportion comparison methods cannot compare results with differing numbers of endmembers.
3) Previous methods require solving, outright, the correspondence problem between endmember spectra.
4) Previous methods only compare endmembers or proportion values, not both simultaneously.

To overcome these limitations, the Earth Movers Distance (EMD) [12] is explored herein as a mechanism to help simultaneously compare two sets of endmember spectral signatures and corresponding proportion values. In other words, the EMD provides the new functionality to be able to compare endmember and proportion *sets*. The EMD is proposed as a method for *comparison* of endmember and proportion sets (and not necessarily evaluation.) Comparison approaches (like those discussed in the cluster validity and cluster comparison literature [13]–[15]) allow us to identify trends in the data and the processing of the data (e.g., similarities in results across endmember and proportion estimation algorithms). The proposed EMD approach has the following advantages:

1) EMD does not require an outright solution to the difficult correspondence problem between sets of endmembers. Instead, a soft correspondence problem is calculated and used with the concept of ground distance for the EMD.
2) EMD can compare results with different number of endmembers.
3) EMD compares BOTH endmember and proportion values.
4) EMD is flexible as it can be adapted to focus on particular endmember features through appropriate selection of *ground distance*.

A review of commonly used methods for comparing endmember spectral signatures and proportion values is provided in the following sub-sections. Section II is a review of EMD. Section III describes the proposed EMD method to compare sets of endmembers and proportion values. Section IV includes experimental results using both simulated and measured hyperspectral data. Finally, Section V discusses future work.

A. Previous Methods for Endmember Comparison

Spectral angle distance (SAM) [16], [17], spectral information divergence (SID) [18] and squared Euclidean distance (SED) are common proximity measures for comparing endmember spectra. SAM compares endmembers by calculating the angle between two endmember spectra, $\mathbf{x}$ and $\mathbf{y}$, as

$$\mathrm{SAM}(\mathbf{x},\mathbf{y}) = \arccos\left(\frac{\langle \mathbf{x},\mathbf{y}\rangle}{\|\mathbf{x}\|_2^2\|\mathbf{y}\|_2^2}\right). \tag{1}$$

SID compares endmembers using the Kullback-Leibler Divergence between the two endmember spectra,

$$\mathrm{SID}(\mathbf{x},\mathbf{y}) = D(\mathbf{x}\|\mathbf{y}) + D(\mathbf{y}\|\mathbf{x}) \tag{2}$$

where

$$D(\mathbf{x}\|\mathbf{y}) = \sum_{i=1}^{D} x_i \log\left(\frac{x_i}{y_i}\right). \tag{3}$$

SED has also been used in the literature to compare two endmember spectral signatures,

$$\mathrm{SED}(\mathbf{x},\mathbf{y}) = \|\mathbf{x}-\mathbf{y}\|_2^2. \tag{4}$$

These proximity measures can be used to compute a distance between two endmember spectral signatures. If ground truth is available (such as a signature from a spectral library for a material known to be found in a scene), an estimated endmember spectral signature can be evaluated by using one or all of these methods to compare to the ground truth spectral signature. However, provided two sets of endmember spectral signatures, e.g., all of the endmembers estimated for a scene and several ground truth signatures from a spectral library, the correspondence problem of mapping two different sets of endmembers to each other must be solved by the user prior to computing SAM, SID or SED between each pair of endmembers. Furthermore, the correspondence method used (such as an ad hoc approach or methods like the Hungarian algorithm [19]) very often significantly effects the overall results. Also, as these methods measure distance between pairs of endmember signatures, they cannot address results with different numbers of endmembers and, as a result, some ad hoc approach must be taken when using SAM, SID, or SED to compare sets of endmembers with differing numbers of endmembers. Finally, these approaches only compare two endmember spectral signatures. They do not take into account corresponding estimated proportions for a data set.

B. Previous Methods for Proportion Comparison

Estimated proportion values are often evaluated or compared using SED between two vectors of proportion values for a pixel. However, when comparing two sets of proportion values, the endmember to which each proportion corresponds should be taken into account. Thus, the proportion vectors must be sorted appropriately before comparison. In other words, it is not sufficient to compare two proportion vectors to each other without first solving the correspondence problem between the corresponding endmember sets to ensure that the correct proportion values from the two vectors are being compared. Furthermore, as SED is only defined for two vectors of equal length, this approach cannot be used to compare proportion values of different length (i.e., a different number of endmembers).

II. Earth Movers Distance

Traditionally, the EMD has been used to compare histograms. However, a number of applications have explored it for distributions and even sets of descriptors. EMD has been used for a number of applications including image analysis [20], visual tracking [21], dimensionality reduction [22], and news story tracking [23]. Also, variations have been developed for efficiency [24] and special applications [25].

The EMD between $h_1 = \{\mathbf{E},\mathbf{p}\}$ and $h_2 = \{\mathbf{B},\mathbf{q}\}$ where $\mathbf{E}$ and $\mathbf{B}$ are matrices of size $D \times M$ and $D \times N$, $\mathbf{e}_m$ is the center of the mth bin and the mth column in $\mathbf{E}$, the ith row and jth column of $\mathbf{E}$ (or $\mathbf{B}$) is the ith dimension of the jth bin center, and $\mathbf{p}$ and $\mathbf{q}$ are vectors containing the corresponding bin counts, is computed by first minimizing the objective function in (5) subject to the constraints in (6) to (9). This optimization problem is a linear programming problem. The objective function is

$$\mathrm{WORK}(\mathbf{E},\mathbf{B},\mathbf{p},\mathbf{q},\mathbf{f}) = \sum_{m=1}^{M}\sum_{n=1}^{N} d_{mn} f_{mn}, \tag{5}$$

where d_{mn} is the *ground distance* between bin centers $\mathbf{e}_m$ and $\mathbf{b}_n$, p_m is the count for bin center $\mathbf{e}_m$, and q_n is the bin count corresponding to center $\mathbf{b}_n$. Equation (5) is minimized by finding the optimal *flow* $\mathbf{f}$, with respect to the constraints

$$f_{mn} \geq 0 \quad 1 \leq m \leq M, 1 \leq n \leq N, \tag{6}$$

$$\sum_{n=1}^{N} f_{mn} \leq p_m \quad 1 \leq m \leq M, \tag{7}$$

$$\sum_{m=1}^{M} f_{mn} \leq q_n \quad 1 \leq n \leq N, \tag{8}$$

$$\sum_{m=1}^{M}\sum_{n=1}^{N} f_{mn} = \min\left(\sum_{m=1}^{M} p_m, \sum_{n=1}^{N} q_n\right). \tag{9}$$

The *ground distance* between $\mathbf{e}_n$ and $\mathbf{b}_m$, d_{mn}, is the pair-wise distance or dissimilarity between the two bin centers. The minimization of (5) can be interpreted as the minimum cost for transforming one histogram, $\mathbf{p}$, into the other, $\mathbf{q}$, given the bin centers (and the distances between the bin centers) to which they correspond. Intuitively, the EMD can be thought of as follows. Imagine that the two histograms are piles of sand or earth. Then the distance between the two piles can be thought of as how far the grains of sand have to be moved to make one pile be transformed into the other. That is, the EMD is the minimal total ground distance traveled weighted by the amount of sand moved.

TABLE I
RUN TIMES WITH VARYING DATA SIZES (IN SECONDS) THESE EXPERIMENTS WERE RUN ON A MACBOOK PRO WITH 2.3 GHZ INTEL CORE I7 PROCESSOR AND 8 GB 1333 MHZ DDR3 RAM

	$M=2$	$M=6$	$M=8$
$N_x=100$	0.001	0.001	0.001
$N_x=1000$	0.010	0.012	0.014
$N_x=10000$	0.099	0.116	0.138

Once the optimal $\mathbf{f}^*$ is found, which minimizes (5), the EMD is calculated as

$$\mathrm{EMD}(\mathbf{f}^*,\mathbf{E},\mathbf{B},\mathbf{p},\mathbf{q})=\frac{\sum_{m=1}^{M}\sum_{n=1}^{N}f_{mn}^*d_{mn}}{\sum_{m=1}^{M}\sum_{n=1}^{N}f_{mn}^*}. \tag{10}$$

As the optimization task is a linear programming problem, any linear programming approach may be applied such as interior-point methods or the simplex algorithm [26]. Each linear programming method has its own associated average and worst-case computational complexity. The proposed EMD approach (as described in Section III) requires solving a linear programming problem for each pixel, and thus, the approach is linear in terms of the number of pixels. The computational complexity of the proposed approach is also constant in terms of data dimensionality. The largest driving factor for computation time is the length of each histogram (or, in the case of the proposed method, the number of endmembers in each set) and the number of pixels. For illustration, the proposed EMD approach was applied to data sets with $N_x=100, 1000$, and 10000 where N_x is the number of data points and with $M=2, 6$, and 8 where M is the length of each histogram using the implementation of the EMD algorithm found in [27]. The resulting run times with the varying data sizes are shown in Table I. Furthermore, computationally efficient approximations have been developed for application to the EMD. In particular, Shirdhonkar and Jacobs developed an approximate technique based on wavelets that runs in linear time, $O(M)$ in which M is the length of the histogram [28]. As the problem is a convex linear programming problem, any standard linear programming approach will find the globally optimal solution. However, in the case of an approximation approach, such as that presented by Shirdhonkar and Jacobs, the behavior of the EMD may change due to possible inaccuracies in the estimation of f^*. The characteristics of the EMD when using their approximation approach is discussed by Shirdhonkar and Jacobs in their corresponding paper [28].

III. EMD FOR ENDMEMBER AND PROPORTION COMPARISON

In this paper, the EMD is proposed as a method to compare sets of endmembers and proportion values. The EMD can be used to compare two endmember sets and proportion vectors, $\{\mathbf{E},\mathbf{p}\}$ and $\{\mathbf{B},\mathbf{q}\}$, by using endmembers in place of histogram bin centers and proportion vectors in place of the histogram bin counts and minimizing (5) and, then, computing (10). Thus, in the proposed method, $\mathbf{E}$ is a matrix of estimated endmember spectra where the ith column, $\mathbf{e}_i$, is the ith endmember in this set. Similarly, $\mathbf{B}$ is a matrix of estimated endmember spectral where the ith column, $\mathbf{b}_i$, is the ith endmember in this set.

Equation (10) calculates the EMD between two proportion vectors (for a single data point) given two sets of endmembers. A single measure of dissimilarity for the entire data set can be computed as an appropriate aggregation of EMD values between the two unmixing results over all pixels in the hyperspectral data, e.g.,

$$\mathrm{EMD}_{\mathrm{tot}}(\mathbf{F}^*,\mathbf{E},\mathbf{B},\mathbf{P},\mathbf{Q})=\sum_{i=1}^{N_x}\mathrm{EMD}(\mathbf{f}_i^*,\mathbf{E},\mathbf{B},\mathbf{p}_i,\mathbf{q}_i), \tag{11}$$

where N_x is the total number of pixels in the hyperspectral data, $\mathbf{p}_i$ is the proportion vector from $\mathbf{P}$ for the ith data point, and $\mathbf{q}_i$ is the proportion vector from $\mathbf{Q}$ for the ith data point. Note that if the proportions in both $\mathbf{P}$ and $\mathbf{Q}$ were found using a fully constrained unmixing method, then the constraint in (9) should be restated as $\sum_{m=1}^{M}\sum_{n=1}^{N}f_{mn}=1$.

The EMD does not transform one endmember set into the other. Instead, the EMD begins by solving a "soft" correspondence problem between the endmember sets. The magnitude of the EMD, and therefore its aggregated result, is governed by the value of the pair-wise ground distance between the endmembers and the similarity of the corresponding proportion values. In essence, the EMD is minimizing the (generally, non-linear) pair-wise ground distance between endmembers subject to constraints based on proportion values. More specifically, our EMD approach has the following advantages:

1) *It does not require the outright difficult solution to a correspondence problem between sets of endmembers:* The EMD employs a *soft* endmember correspondence by solving the corresponding transportation problem [12] given the ground distance between each pair of endmembers. This is a more flexible and simpler approach to comparing endmember sets as opposed to determining a hard one-to-one correspondence between pairs of endmember spectral signatures. The approach is simplified since each endmember does not need to be strictly associated with only one corresponding endmember from the other set. Instead, endmembers have partial correspondence as determined by their relative ground distances.
2) *It can be used to compare results with different numbers of endmembers:* Since a soft correspondence between endmembers is used, the EMD can compare sets with differing numbers of endmembers. Due to this soft correspondence, the EMD can inherently handle differing numbers of endmembers without any additional steps.
3) *It takes into account both endmember and proportion values during comparison:* When computing the EMD, not only are the ground distances between pairs of endmembers considered but the corresponding proportions are also factored in. Therefore, the EMD computes a single distance values that takes into account the similarity between the endmember sets and their corresponding proportions simultaneously.

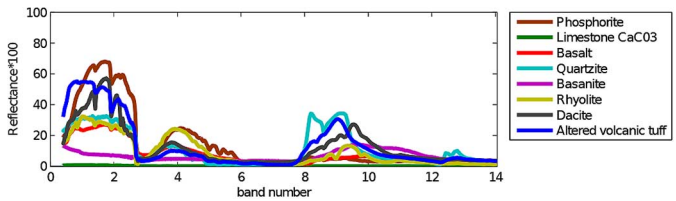

Fig. 1. True endmembers from the ASTER spectral library used to generate 500 simulated hyperspectral data points.

4) *It can be adapted to focus on particular endmember features by selecting an appropriate ground distance:* The ground distance used to compute EMDtot for hyperspectral data can be SED, SAM, SID or another appropriate measure. Furthermore, a ground distance can be defined to focus on particular wavelengths, spectral shape, etc. such that the EMD focuses on specific features of interest in the endmember spectral signatures. For example, SED takes into account differences in both magnitude and spectral shape; SAM compares the spectral angle between endmembers; and SID computes the information divergence between endmembers. The ability to modify the ground distance allows the proposed approach to capture the important characteristics of a hyperspectral data set under consideration.

IV. Experimental Results

In the following sub-sections, experimental results are shown using simulated and measured hyperspectral data. Simulated data is often used to evaluate unmixing and endmember estimation methods in the literature since the true endmembers and proportions are known (which is generally not the case for measured hyperspectral data). Using simulated data, several experiments are conducted to illustrate some of the properties of the proposed EMD approach. Following the simulated data results, results on measured hyperspectral imagery are presented in which the EMD is used to compare and cluster endmember estimation and spectral unmixing results obtained using multiple algorithms.

A. Simulated Data Results

For the simulated data experiments, data is generated using the eight spectra from the ASTER spectral library [29] shown in Fig. 1. Proportion values are generated using the sampling scheme described in Algorithm 1. This approach is taken to generate more realistic simulated data in which the entire set has a total of eight endmembers but individual pixels are composed of only a subset with proportion values sampled from unique Dirichlet distributions. A Dirichlet distributions is defined only over non-negative values that sum to one which are requirements needed for proportion values. Each data set generated has 500 data points.

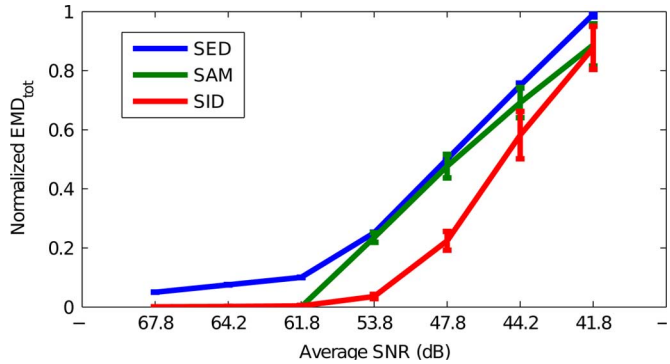

Fig. 2. This plot shows that the EMD gives the best result on endmembers with the lowest error (as desired). Each solid line is the mean EMD over all runs at that noise level using either SAM, SED or SID ground distances. The error bars represent ± 1 standard deviation. The $\mathrm{EMD}_{\mathrm{tot}}$ values for each ground distance were normalized to range between 0 and 1 such that the results across the three ground distances could be shown on the same axes. The values were normalized by dividing by the maximum $\mathrm{EMD}_{\mathrm{tot}}$ value computed for each ground distance in this experiment. The average standard deviation for each plot (SAM, SED, and SID) across all SNR values is 0.004, 0.024, and 0.026, respectively.

Algorithm 1 Simulated Data Generation

for $j \leftarrow 1$ to N_x **do**
  Sample m_j from multinomial distribution with mean $\frac{1}{M}$ where M is the total number of endmembers and m_j is the number of endmembers found in pixel j
  Sample m_j endmembers, $\mathbf{E}_j$, uniformly from the full set of M endmembers
  Sample α_i for $i = 1, \ldots, m_j$ from an exponential distribution with a mean of 2.
  Sample proportion vector $\mathbf{p}_j$ (for pixel j) from a Dirichlet distribution with concentration parameters $\alpha = [\alpha_1, \ldots, \alpha_{m_j}]$ sampled in the previous step
  Set $\mathbf{x}_j = \mathbf{p}_j \mathbf{E}_j$
end for

1) Varying Endmember Noise: First, the ability of the EMD to operate well in light of endmember error is empirically explored. In particular, varying amounts of noise is applied to the true endmembers and the resulting noisy endmembers are compared to the true endmembers to gauge the effects of endmember noise on the resulting EMD calculations. Proportion values are held fixed to the true value during this experiment. The resulting signal to noise ratio, SNR, on the noisy endmembers ranges from 67.8 dB to 41.8 dB over 7 noise levels. The noise levels are varied by adjusting the variance on the Gaussian used to generate the random noise from 0.005 to 0.1 with increments of 0.025. Ten noisy endmembers sets are generated at each noise level and the EMD is computed for each of the 10 runs. As shown in Fig. 2, the EMD appropriately gives the smallest EMD to the least noisy endmembers using any of the ground distances considered (SED, SID or SAM). As the endmembers become more noisy, the EMD increases which is a desirable result as it indicates that when estimated endmembers have larger error or noise, the EMD distance to the true values increase.

Although shown empirically here, the EMD increases as the error or noise between endmember sets increase. This result is

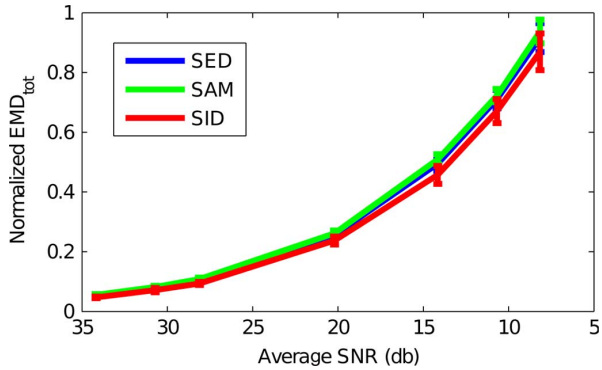

Fig. 3. This plot shows that the EMD gives the best result on the proportions with the lowest error (as desired). Each solid line is the mean EMD over all runs at that noise level using either SAM, SED or SID ground distances. The error bars represent ± 1 standard deviation. The $\mathrm{EMD}_{\mathrm{tot}}$ values for each ground distance were normalized to [0, 1] such that the results across the three ground distances could be shown on the same axes. The values were normalized by dividing by the maximum $\mathrm{EMD}_{\mathrm{tot}}$ value computed for each ground distance in this experiment. The average standard deviation for each plot (SAM, SED, and SID) across all SNR values is 0.017, 0.013, and 0.022, respectively.

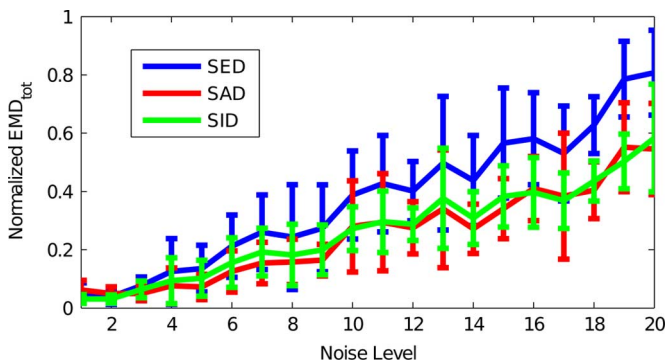

Fig. 4. This plot shows that the EMD gives the best result on data with the lowest error (as desired). The solid line is the mean $\mathrm{EMD}_{\mathrm{tot}}$ over all runs at that noise level. The error bars represent ± 1 standard deviation. The $\mathrm{EMD}_{\mathrm{tot}}$ values for each ground distance were normalized to [0, 1] such that the results across the three ground distances could be compared and shown on the same axes. The values were normalized by subtracting the minimum $\mathrm{EMD}_{\mathrm{tot}}$ value and dividing by the maximum $\mathrm{EMD}_{\mathrm{tot}}$ value found in this experiment. The average standard deviation for each plot (SAM, SED, and SID) across all SNR values is 0.231, 0.175, and 0.346, respectively.

expected as the EMD is a metric when: (1) the ground distance used is a metric and (2) the sum of the proportion values from each set are equal (i.e., sum to a constant value). Of particular note, if the ground distance used is a metric and the proportions are constrained to sum to one, then the EMD solution is equivalent to the Mallow's distance. However, the EMD approach allows for the flexibility to accommodate non-metric ground distances and proportion values that are not constrained to sum to one [14].

2) Varying Proportion Error: In this experiment, the EMD is examined for the case with proportion values with increasing amounts of noise/error. The EMD was computed using fixed true endmember values and noisy proportion values at 7 noise-levels (ranging SNR from 36 dB to 8 dB) for 10 runs. As shown in Fig. 3, the EMD once again correctly gives the smallest EMD for the least noisy proportion values. Again, this is attributed to the metric properties of the EMD and our aggregation operation.

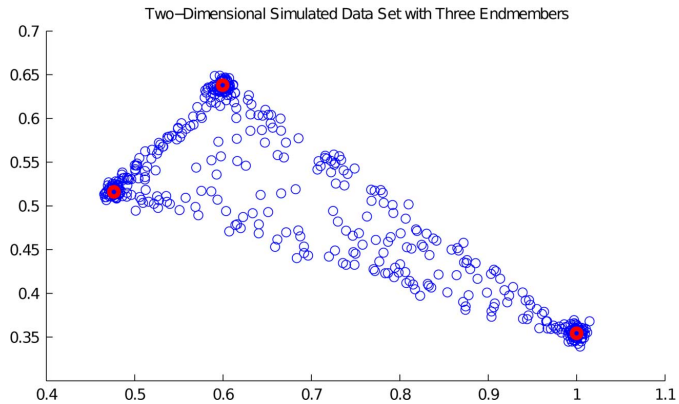

Fig. 5. Simulated data used in (c) Case 3 of the varying number of endmembers experiment. Proportion values were generated using the method described in Algorithm 1. Gaussian zero-mean random noise was added.

3) Variation of Data Noise Levels: In this experiment, the EMD between true endmember and proportion values and values estimated from data with increasing levels of noise is explored. In particular, the amount of noise added to the data generated using the method described in Algorithm 1 is varied, endmembers and proportions are estimated using the Iterated Constrained Endmembers (ICE) algorithm [30] algorithm, and, then, these resulting endmembers and proportions are compared to the true values to gauge the effects of noise on the resulting EMD calculations. In these experiments, the number of endmembers estimated was held fixed to the true value. Two types of noise were added to the simulated data set: zero-mean Gaussian noise and spectral noise. The spectral noise was noise added to the data to simulate the inclusion of some unknown spectral signature in the data. The resulting signal to noise ratio, SNR, on the noisy data ranged from 83.5 dB to 58.5 dB over 20 noise levels. Ten simulated data sets are generated at each noise level and the EMD is computed for each of the 10 runs of the ICE algorithm. The ICE algorithm was applied to the data in the original dimensional space with random initialization. This experiment was repeated for three different ground distance options: SED, SAM and SID. As shown in Fig. 4, the EMD appropriately gives the smallest EMD to the least noisy data results because, as you would expect, the most accurate endmember and proportion estimates come from the data with the least noise.

The ICE algorithm is dependent on parameter settings and initialization and may not always provide the globally optimal results for every input data set. Thus, as shown in Fig. 4, EMD values do not strictly increasing with increasing noise levels. This is a result of the endmember estimation and spectral unmixing algorithm not the EMD (as illustrated by the behavior of the EMD in the previous two experiments).

4) Variation of Endmember Scale: Several endmember estimation and spectral unmixing algorithms have recently explored the issue of representing spectral variability of a material [31]. These include methods that estimate endmembers and unmix using *endmember bundles* [32], *endmember distribution* approaches [33], [34], and others that represent or discuss spectral variability during analysis [13], [35]. In order to investigate the effect of spectral variability in the proposed approach, an

TABLE II
ASTER SIMULATED DATA WITH SCALED ENDMEMBERS $\mathrm{EMD_{tot}}$ VALUE (± 1 STD. DEV. OVER 10 RUNS) BETWEEN SCALED AND TRUE ENDMEMBERS WITH FIXED PROPORTION VALUES

Scale	SED	SAM	SID
1.0	$7.1 \times 10^{-5} \pm 2.1 \times 10^{-4}$	$4.1 \times 10^{-7} \pm 5.0 \times 10^{-6}$	$1.8 \times 10^{-3} \pm 3.9 \times 10^{-4}$
0.5	$1.3 \times 10^{5} \pm 2.3 \times 10^{3}$	$3.6 \times 10^{-7} \pm 3.1 \times 10^{-6}$	$2.0 \times 10^{6} \pm 3.5 \times 10^{4}$
0.25	$1.9 \times 10^{5} \pm 3.3 \times 10^{3}$	$3.7 \times 10^{-7} \pm 3.7 \times 10^{-6}$	$6.0 \times 10^{6} \pm 8.8 \times 10^{4}$
0.1	$2.3 \times 10^{5} \pm 3.3 \times 10^{3}$	$3.8 \times 10^{-7} \pm 2.7 \times 10^{-6}$	$1.2 \times 10^{7} \pm 1.6 \times 10^{5}$

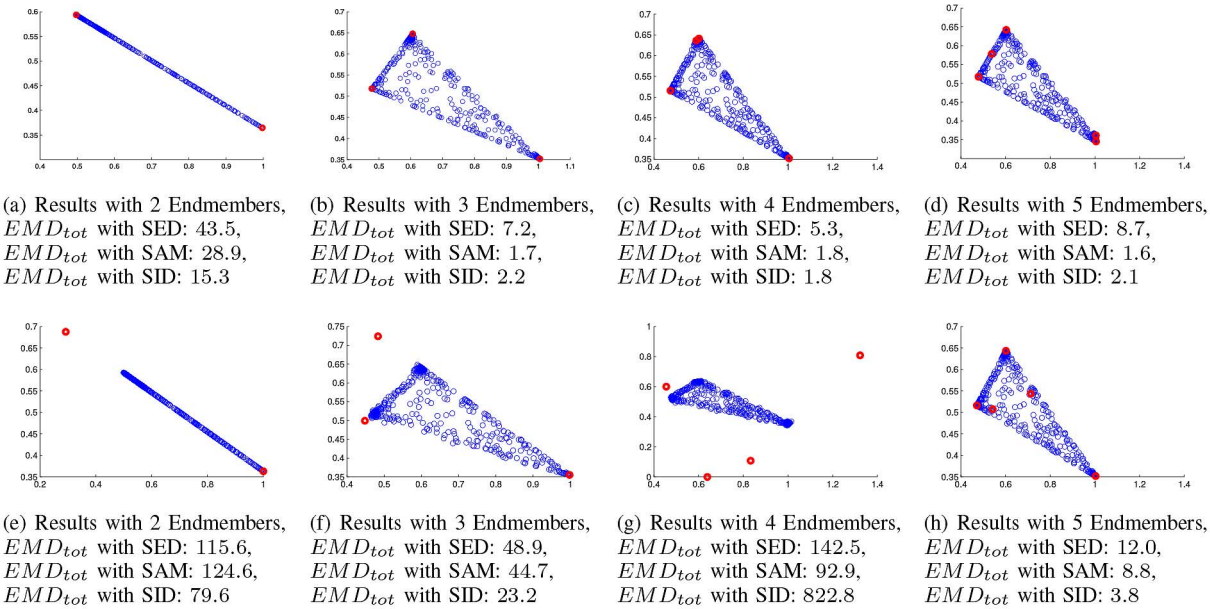

(a) Results with 2 Endmembers, EMD_{tot} with SED: 43.5, EMD_{tot} with SAM: 28.9, EMD_{tot} with SID: 15.3

(b) Results with 3 Endmembers, EMD_{tot} with SED: 7.2, EMD_{tot} with SAM: 1.7, EMD_{tot} with SID: 2.2

(c) Results with 4 Endmembers, EMD_{tot} with SED: 5.3, EMD_{tot} with SAM: 1.8, EMD_{tot} with SID: 1.8

(d) Results with 5 Endmembers, EMD_{tot} with SED: 8.7, EMD_{tot} with SAM: 1.6, EMD_{tot} with SID: 2.1

(e) Results with 2 Endmembers, EMD_{tot} with SED: 115.6, EMD_{tot} with SAM: 124.6, EMD_{tot} with SID: 79.6

(f) Results with 3 Endmembers, EMD_{tot} with SED: 48.9, EMD_{tot} with SAM: 44.7, EMD_{tot} with SID: 23.2

(g) Results with 4 Endmembers, EMD_{tot} with SED: 142.5, EMD_{tot} with SAM: 92.9, EMD_{tot} with SID: 822.8

(h) Results with 5 Endmembers, EMD_{tot} with SED: 12.0, EMD_{tot} with SAM: 8.8, EMD_{tot} with SID: 3.8

Fig. 6. Endmembers and reconstructed data points (computed using the estimated endmembers and proportion values) estimated from two runs the ICE algorithm with random initialization. $\mathrm{EMD_{tot}}$ was computed between the estimated endmembers and proportion values found on each run and the true values used to generate the data. Two sets of results are shown for each number of endmembers estimated. One set of results had relatively small $\mathrm{EMD_{tot}}$ values and one set of results had relatively large $\mathrm{EMD_{tot}}$ values.

experiment where endmember scale was varied was conducted. The scaled endmembers were compared using EMD to the original unscaled endmembers with fixed proportion values. Results are shown in Table II. As can be seen, the EMD result with the SAM ground distance was unaffected by scale with values close to zero (variation coming from noise added to the data). In contrast, the $\mathrm{EMD_{tot}}$ values associated with SED or SID increase with larger changes in scale. This was to be expected as SAM compares endmembers using spectral shape (and disregards scale) in contrast to the SED and SID ground distances.

The results of this experiment illustrate the flexibility of the proposed EMD comparison method. Different ground distances can be used to emphasize certain features between endmember spectral signatures that are important for a given application. For example, if spectral shape is considered important but scale can be disregarded, then SAM is the appropriate ground distance to be used. Beyond SAM, SED, or SID, ground distances that emphasize certain features in endmember spectral signatures can be constructed and used within the proposed EMD comparison method such as distances with band weights (i.e., some spectral bands are of more importance than others), etc.

5) Varying the Number of Endmembers: In this section, the EMD is investigated over varying numbers of estimated endmembers. This section is significant since no other methods previously used to evaluate unmixing results are able to inherently address different numbers of endmembers. This advantage goes beyond manually solving correspondence for equal numbers of endmembers. To illustrate EMD behavior, consider the following special cases.

a) Case 1: Duplicate Endmembers: In this case, two sets of endmembers and proportion values are compared where, in the first set, there are three endmembers (Phosphorite, Limestone, and Basalt from the ASTER spectral library) and one proportion vector equal to $[0.2, 0.6, 0.2]$. This first set is compared to a second set in which there are four endmembers of which two are duplicate Limestone endmembers, (Limestone, Phosphorite, Limestone and Basalt, respectively) with one proportion vector equal to $[0.2, 0.2, 0.4, 0.2]$. Thus, in this case, the second set of values simply split the proportions associated to Limestone across two duplicate Limestone endmembers. The resulting EMD values using SED, SAM and SID ground distances are 9.7×10^{-12}, 6.0×10^{-13}, and 7.4×10^{-11}, respectively. All of these values are effectively zero. This illustrates that the EMD approach appropriately takes into account endmember spectral shape, duplicate endmembers, and their corresponding proportion values when comparing sets of endmembers.

b) Case 2: Unused Endmembers: In this case, two sets of endmembers and proportion values are compared where, in the first set, there are three endmembers (Phosphorite, Limestone,

and Basalt from the ASTER spectral library) and one proportion vector equal to $[0.3, 0.3, 0.4]$. This first set is compared to a second set in which there are four endmembers (Phosphorite, Limestone, Basalt, and Quartzite, respectively) with one proportion vector equal to $[0.3, 0.3, 0.4, 0]$. Thus, in this case, the second set of values are equivalent to the first set except with inclusion of a fourth endmember which has a zero corresponding proportion value. The resulting EMD values using SED, SAM and SID ground distances are 1.3×10^{-15}, 3.6×10^{-15}, and 3.1×10^{-13}, respectively. Again, all of these values are effectively zero. This illustrates that the EMD approach appropriately disregards additional endmembers when they are not being used to represent the data (as shown with proportion values of zero).

c) Case 3: Varying Number of Estimated Endmembers and Proportions: In this case, the EMD was applied to endmember and proportion results obtained from ICE over two-dimensional simulated data. The proportion values for this data was generated using the method described in Algorithm 1. Two-dimensional simulated data was generated such that the results can be visualized and shown here. The simulated data used is shown in Fig. 5.

ICE was applied to this simulated data set used to estimate $2, \ldots, 5$ endmembers. ICE was applied because the method can be used to estimate more endmembers than the dimensionality of the data. Although having more endmembers than the dimensionality of the data is not standard for hyperspectral image analysis, the experiment was conducted in this way allows visualization of the results and comparison of these results to the resulting $\mathrm{EMD}_{\mathrm{tot}}$ values for the data set. ICE was run with parameter $\mu = 0.001$ and random initialization. The endmembers and reconstructed data points (computed using the estimated endmembers and proportion values) estimated by ICE are shown in Fig. 6. $\mathrm{EMD}_{\mathrm{tot}}$ was computed between the estimated endmembers and proportion values found on each run and the true values used to generate the data and is shown in the caption of each sub-figure in Fig. 6.

By examining the results shown in Fig. 6, it can be seen that the proposed EMD approach takes into account the overall similarity or accuracy of the spectral unmixing results during comparison and simply having the correct number of endmembers estimated is insufficient to have a small $\mathrm{EMD}_{\mathrm{tot}}$ value. For example, the spectral unmixing results shown in Fig. 6(c) has four endmembers estimated (where the true value contains three endmembers). However, two of the estimated endmembers in this result are nearly identical. Thus, they EMD will behave similar to as illustrated in the previous duplicate endmember experiment and the resulting $\mathrm{EMD}_{\mathrm{tot}}$ value is not penalized with the inclusion of an additional endmember. In contrast, the results in Fig. 6(f) have relatively large $\mathrm{EMD}_{\mathrm{tot}}$ value despite estimating the correct number of endmembers; this is a result of one of the three endmembers being poorly estimated. This result emphasizes the the EMD is not a model selection approach but, instead, simply computes a distance between two endmember and proportion sets.

6) Comparing Only Endmember Values: The EMD is proposed as a method to *simultaneously* compare endmember and proportion values (as a pair). However, in some cases, one may want to determine whether increased EMD values are a result of differences in proportion values, endmember values, or a combination of the two. In these cases, the EMD can be used to compare endmember values only with the approach described in Algorithm 2. Namely, to compare two sets of endmembers using the EMD, identical proportion vectors of length M with all values equal to $(1)/(M)$ can be constructed. Then, using these proportion vectors, the EMD can be computed to compare the endmember values only. If the resulting EMD (with the proportion vectors constructed as described) is zero, then the sets of endmembers are identical and any differences identified by the full EMD are the result of differences in the proportion values only. If the EMD value with the constructed proportion vectors is non-zero, then the endmembers differ. Note, however, with differing endmembers, the meaning of any associated proportion values will differ as well.

Algorithm 2 Comparing Two Endmember Sets (without considering any proportion values)

1: **Input:** Endmember Sets: $\mathbf{E}$, $\mathbf{B}$ of size M and N
2: Construct proportion vector of length M as $\mathbf{p}_1 = \left[\frac{1}{M}, \ldots, \frac{1}{M}\right]$
3: Construct proportion vector of length N as $\mathbf{p}_2 = \left[\frac{1}{N}, \ldots, \frac{1}{N}\right]$
4: **Return:** $EMD(f^*, \mathbf{E}, \mathbf{B}, \mathbf{p}_1, \mathbf{p}_2)$ where f^* is found as described in Section II

To examine this, one set of eight endmembers was composed from the spectra from the ASTER spectral library shown in Fig. 1. The EMD was computed between this set and itself (i.e., identifical endmember sets) using the approach described in Algorithm 2. Then, this endmember set was compared to itself with increasing zero-mean Gaussian random noise added (using the approach in Algorithm 2). The results are shown in Fig. 7(a).

For comparison, the difference between these endmember sets were also computed using SAM, SED, and SID. However, SAM, SED, and SID were designed to only compare one pair of endmembers at a time. Therefore, they cannot address the comparison of a sets of endmembers without an extension. Thus, to perform this comparison, the SAM, SED and SID approaches were extended using an ad-hoc greedy strategy. Each pair of endmembers with the smallest pairwise SAM, SED, or SID value were identified. These endmembers were remove from the set and, then, the next pair of endmembers with the smalled pairwise SAM, SED, or SID value was identified. This was repeatedly iteratively until every endmember was paired off with an endmember from the other set. Then the SAM, SED, and SID values sum across all identified pairs for the final score. *Note, this ad-hoc greedy approach for SAM, SED, and SID cannot be applied to endmembers of different sizes (as it required identifing one matching endmember from the other set) nor does this approach take into account proportion values*. The comparison results are shown in Fig. 7(b). Note that the results are identical between the extended SAM, SED and SID approaches and the EMD with the respective ground distances. Thus, in cases in which only endmembers are considered *and there is a clear one-to-one correspondence between the two sets of endmembers*, the EMD behaves exactly as its respective ground dis-

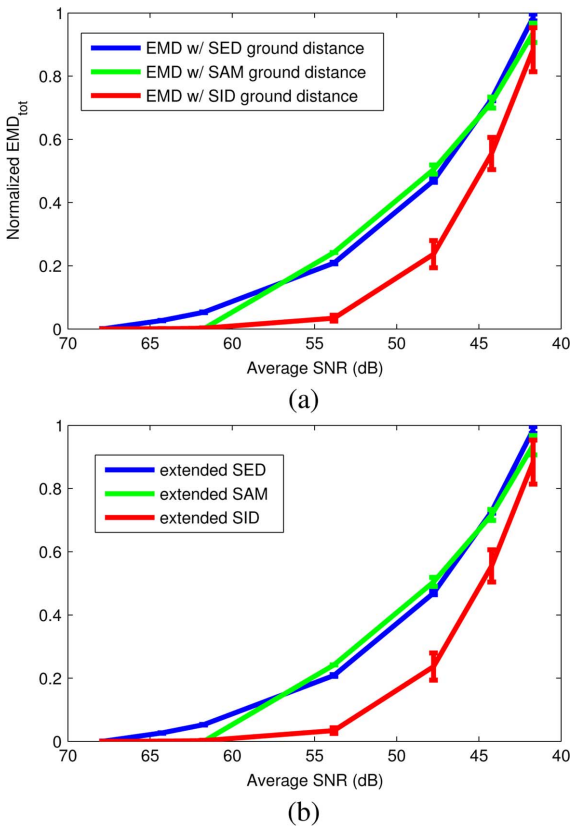

Fig. 7. (a) This plot compares EMD (with SED, SAM and SID ground distance) results for endmember only experiments (as described in Algorithm 2 with increasing noise levels. Each solid line is the mean EMD over ten runs at that noise level using either SAM, SED or SID ground distances. The error bars represent ± 1 standard deviation. The $\mathrm{EMD}_{\mathrm{tot}}$ values for each ground distance were normalized to [0, 1] such that the results across the three ground distances could be shown on the same axes. The values were normalized by dividing by the maximum $\mathrm{EMD}_{\mathrm{tot}}$ value computed for each ground distance in this experiment. The average standard deviation for each plot (SAM, SED, and SID) across all SNR values is 0.004, 0.009, and 0.025, respectively. (b) This plot shows the endmember only experiment results with extended version of SAM, SED and SID (as described in the text). Each solid line is the mean SAM, SED or SID value over ten runs at that noise level. The error bars represent ± 1 standard deviation. The values for each distance were normalized to [0, 1] such that the results could be shown on the same axes. The values were normalized by dividing by the maximum value computed for each distance in this experiment. The average standard deviation for each plot (SAM, SED, and SID) across all SNR values is 0.004, 0.009, and 0.025, respectively.

tance. However, the EMD provides a framework in which to extend these ground distances to be able to compare endmember setsb of varying sizes along with their corresponding proportion values which is beyond the capabilities of this ad-hoc greedy approach.

B. Comparison of Spectral Unmixing Results on Pavia

The experiments on the simulated data demonstrate that the EMD is effective for evaluating spectral unmixing results when ground truth is available and illustrate some of the properties of the EMD. However, pixel-level proportion ground truth is rarely known for measured hyperspectral data scenes. In these cases, spectral unmixing results cannot be evaluated in comparison to true values given that a full ground-truth is unavailable. However, the EMD can compare endmember estimation and spectral

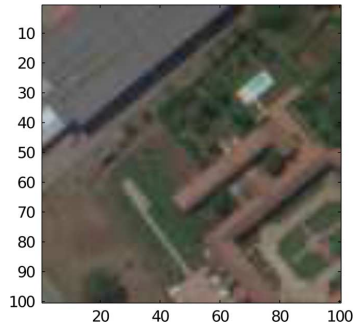

Fig. 8. Sub-image of the ROSIS Pavia University data set (using wavelengths 661.9, 548, and 476 nm to for R, G, and B channels to create the color image) collected over Pavia, Italy.

unmixing results. In the following experiment, the EMD is used to compare results found using three endmember estimation and spectral unmixing algorithms over a range of parameter values.

The measured data set used in this experiment is a subset of the Reflective Optics System Imaging Spectrometer (ROSIS) Pavia University data set collected on July 8, 2002. This hyperspectral data set was collected over an urban area of Pavia, in northern Italy by the ROSIS spectrometer. The image used contains 100×100 pixels with 103 bands. The ROSIS sensor collected data over the 430–850 nm wavelength range at a 4 nm spectral sampling interval. The instantaneous field of view of the sensor is 0.56 mrad with a total field of view with plus or minus 8 degrees. The data shown are in reflectance and was atmospherically corrected by DLR (German Remote Sensing Data Center). Holzwarth, *et al.*, provide more information on the sensor and pre-processing steps [36]. The image contains both natural and urban regions as shown in Fig. 8.

Three spectral unmixing and endmember estimation algorithms were applied to this data set over a range of parameter settings. The algorithms were Vertex Component Analysis (VCA) [37], Iterated Constrained Endmembers (ICE) [30], and Sparsity Promoting ICE [38] (SPICE). The VCA algorithm was applied to the data set with random initialization. The parameter settings were varied such that VCA estimated 3 to 6 endmembers for a total of four runs. Since VCA is strictly an endmember estimation algorithm, proportions were estimated by minimizing the following squared error objective using quadratic programming,

$$J(\mathbf{p}_i) = \left\| \mathbf{x}_i - \sum_{m=1}^{M} \mathbf{e}_m \mathbf{p}_{im} \right\|_2^2 \tag{12}$$

subject to the constraints

$$\sum_{m=1}^{M} p_{im} = 1, \quad p_{im} \geq 0, \tag{13}$$

where $\mathbf{x}_i$ is the ith data point, $\mathbf{e}_m$ is the mth estimated endmember, and p_{im} is the associated proportion value. ICE was also run four times with random initialization. ICE's regularization parameter was fixed at $\mu = 0.001$. The number of endmembers estimated was varied from 3 to 6 endmembers for a total of four runs. SPICE is an extension of ICE algorithm that simultaneously estimates the number of endmembers using a sparsity promoting term on the estimated proportion values. SPICE's

TABLE III
PAIRWISE EMD BETWEEN TWELVE ENDMEMBER ESTIMATION AND SPECTRAL UNMIXING RESULTS FOUND USING VCA, ICE AND SPICE ALGORITHMS ($\times 10^4$). THE LARGEST VALUES PER ROW ARE ITALICIZED AND SMALLEST (EXCLUDING THE DIAGONAL) VALUES PER ROW ARE BOLDED. THE LARGEST, SMALLEST AND MEDIAN VALUES IN THE TABLE ARE UNDERLINED

	VCA, M=3	VCA, M=4	VCA, M=5	VCA, M=6	ICE, M=3	ICE, M=4	ICE, M=5	ICE, M=6	SPICE, Γ=0.1	SPICE, Γ=1	SPICE, Γ=10	SPICE, Γ= 100
VCA, M=3	0.00	0.99	0.79	**0.42**	2.19	1.67	1.93	*2.43*	2.24	1.85	1.41	1.61
VCA, M=4	0.99	0.00	1.04	0.88	1.63	1.10	1.42	*2.09*	2.08	1.45	**0.86**	1.08
VCA, M=5	0.79	1.04	0.00	**0.69**	1.89	1.31	1.70	*2.18*	2.03	1.65	1.07	1.54
VCA, M=6	**0.42**	0.88	0.69	0.00	2.14	1.60	1.86	*2.40*	2.17	1.79	1.34	1.57
ICE, M=3	*2.19*	1.63	1.89	2.14	0.00	**1.10**	1.24	1.43	1.42	1.30	1.34	1.63
ICE, M=4	1.66	1.10	1.31	1.60	1.10	0.00	1.06	*1.68*	1.66	1.26	**0.73**	1.21
ICE, M=5	*1.93*	1.42	1.70	1.86	1.24	1.06	0.00	1.24	1.42	**0.68**	1.18	1.00
ICE, M=6	*2.43*	2.09	2.18	2.40	1.43	1.68	**1.24**	0.00	1.41	1.25	1.79	1.66
SPICE, Γ=0.1	*2.25*	2.01	2.03	2.17	1.42	1.66	1.42	1.41	0.00	**1.23**	1.91	1.77
SPICE, Γ=1	*1.85*	1.45	1.65	1.79	1.30	1.26	**0.68**	1.25	1.23	0.00	1.30	1.25
SPICE, Γ=10	1.41	0.86	1.07	1.34	1.34	**0.73**	1.18	1.79	*1.91*	1.30	0.00	0.82
SPICE, Γ=100	1.61	1.08	1.54	1.57	1.62	1.21	1.00	1.66	*1.78*	1.25	**0.82**	0.00

TABLE IV
PAIRWISE AGGREGATED EMD BETWEEN TWELVE ENDMEMBER ESTIMATION AND SPECTRAL UNMIXING RESULTS FOUND USING VCA, ICE AND SPICE ALGORITHMS. THE LARGEST VALUES PER ROW ARE ITALICIZED AND SMALLEST (EXCLUDING THE DIAGONAL) VALUES PER ROW ARE BOLDED. THE LARGEST, SMALLEST AND MEDIAN VALUES IN THE TABLE ARE UNDERLINED

	VCA, M=3	VCA, M=4	VCA, M=5	VCA, M=6	ICE, M=3	ICE, M=4	ICE, M=5	ICE, M=6	SPICE, Γ=0.1	SPICE, Γ=1	SPICE, Γ=10	SPICE, Γ= 100
VCA, M=3	0.00	0.88	0.76	**0.38**	2.15	1.63	1.91	*2.39*	2.22	1.79	1.36	1.53
VCA, M=4	0.88	0.00	0.91	**0.82**	1.60	1.07	1.38	*2.06*	2.02	1.37	0.83	1.05
VCA, M=5	0.76	0.91	0.00	**0.65**	1.78	1.25	1.61	*2.11*	1.96	1.56	0.98	1.45
VCA, M=6	**0.38**	0.82	0.66	0.00	2.08	1.57	1.83	*2.34*	2.12	1.70	1.32	1.47
ICE, M=3	*2.15*	1.60	1.78	2.08	0.00	**0.97**	1.21	1.40	1.40	1.28	1.24	1.58
ICE, M=4	1.63	1.07	1.25	1.57	0.97	0.00	1.02	*1.66*	1.61	1.21	**0.70**	1.09
ICE, M=5	*1.91*	1.38	1.62	1.83	1.21	1.02	0.00	1.22	1.36	**0.55**	1.12	0.98
ICE, M=6	*2.39*	2.07	2.11	2.34	1.40	1.66	**1.22**	0.00	1.33	1.22	1.68	1.58
SPICE, Γ=0.1	*2.22*	2.02	1.96	2.12	1.40	1.61	1.36	1.33	0.00	**1.13**	1.83	1.73
SPICE, Γ=1	*1.80*	1.37	1.56	1.70	1.28	1.21	**0.55**	1.22	1.13	0.00	1.23	1.23
SPICE, Γ=10	1.36	0.83	0.98	1.32	1.24	**0.70**	1.12	1.68	*1.83*	1.23	0.00	0.81
SPICE, Γ=100	1.53	1.06	1.45	1.47	1.59	1.09	0.98	1.58	*1.73*	1.23	**0.81**	0.00

regularization parameter was also fixed to $\mu = 0.001$. The sparsity promotion parameters was varied, $\Gamma = 0.1, 1, 10, 100$. This resulted in the estimation of 10, 9, 6, 5 endmembers in each experiment, respectively.

After running these algorithms on the Pavia data set with the range of parameter values, the EMD was computed between each pair of results. These pairwise EMD values between the VCA, ICE and SPICE results are shown in Table III.

The following is a qualitative analysis of the similarity between different clusterings as identified by the EMD. Specifically, we explore the extreme cases, i.e., maximum and minimum EMD scores. Figs. 9 and 10 show the proportion maps and the endmembers from the pair of results with the minimum EMD value. When comparing these proportion maps, it can be seen that the first three proportion maps are extremely similar across the two results. The largest difference is where the shadowed and vegetated regions are placed. In the first set of results with VCA, $\mathrm{M} = 3$, the shadow is split among the second and third proportion maps whereas the second set of results, VCA $\mathrm{M} = 6$, has a separate proportion map for shadow. Similarly, the vegetation region is split across the third and fifth maps in the VCA $\mathrm{M} = 6$ results whereas they are grouped in the third proportion map in the VCA $\mathrm{M} = 3$ results. The similarity between these maps can be seen by considering the endmembers as well. Specifically, the second set of results introduces a shadow endmember (cyan) in Fig. 10 as well as an additional vegetation endmember (purple), otherwise, endmember spectral signatures are very similar in shape.

Figs. 11 and 12 show the proportion maps and the endmembers from the pair of results with the maximum EMD value. In this case, the proportion maps and corresponding endmembers are very distinct.

When considering the pairwise EMD scores in Table III, it is noted that hat the VCA $\mathrm{M} = 3$ results are very interesting providing the maximum, median, and minimum EMD score across the full set of results. This indicates, along with the EMD scores for the other spectral unmixing results in this experiment, that the minimum EMD score is not biased towards selecting the same algorithm showing that this approach can compare evenly results across algorithms.

In these results, the range of EMD scores are tabulated and the associated results are investigated. In a case where groups or clusters of endmember and proportion estimation results emerge in the pairwise EMD scores, a host of relational clustering algorithms can be used to identify the similar endmember estimation and spectral unmixing clusters [39]–[41].

C. Aggregated EMD Experiments on the Pavia Data Set

In the EMD approach proposed in Section III, the EMD is directly applied to each pixel in hyperspectral image independently. This results in a, possibly, unique soft matching for each pixel between the endmember sets. This will particularly occur

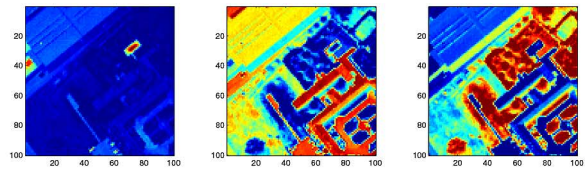

(a) 1: VCA, M = 3, Water (b) 2: VCA, M = 3, Building & Sidewalk (c) 3: VCA, M = 3, Vegetation

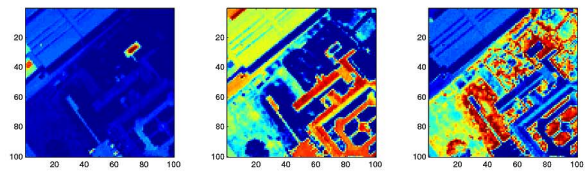

(d) 1: VCA, M = 6, Water (e) 2: VCA, M = 6, Building & Sidewalk (f) 3: VCA, M = 6, Vegetation

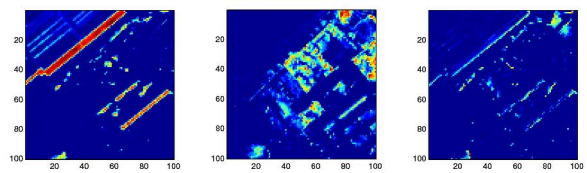

(g) 4: VCA, M = 6, Shadow (h) 5: VCA, M = 6, Grass (i) 6: VCA, M = 6

Fig. 9. Proportion maps from the VCA runs with $\mathrm{M} = 3$ (a)–(c) and $\mathrm{M} = 6$ (d)–(i). This pair of result had the lowest EMD value, thus, these results are the most similar across this experiment. When comparing these proportion maps, it can be seen that the first three proportion maps are extremely similar. The largest difference is where the shadowed and vegetated regions are placed. For example, in the first set of results with VCA, $\mathrm{M} = 3$, the shadow is split among the second and third proportion maps whereas the second set of results, VCA $\mathrm{M} = 6$, has a separate proportion map for shadow.

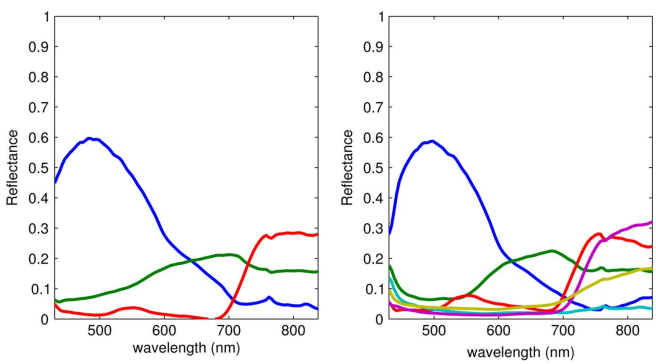

Fig. 10. Endmember spectra from the VCA runs with $\mathrm{M} = 3$ and $\mathrm{M} = 6$. This pair of result had the lowest EMD value, thus, these results are the most similar across this experiment. (a) VCA, $\mathrm{M} = 3$—Blue: Water, Green: Building & Sidewalk, Red: Vegetation, (b) VCA, $\mathrm{M} = 6$—Blue: Water, Green: Building & Sidewalk, Cyan: Shadow, Red: Vegetation, Magenta: Grass.

in cases where a pixel has a zero-value proportion for one endmember and a non-zero values proportion for an endmember in the second set with an extremely small corresponding ground-distance. An advantage of the per-pixel approach is the ability

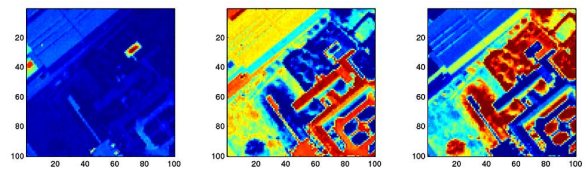

(a) 1: VCA, M = 3, Water (b) 2: VCA, M = 3, Building & Sidewalk (c) 3: VCA, M = 3, Vegetation

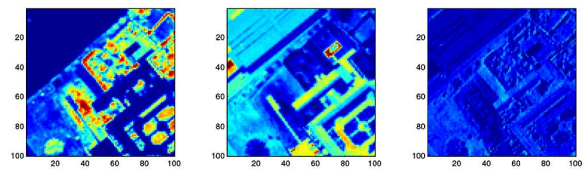

(d) 1: ICE, M = 6 (e) 2: ICE, M = 6 (f) 3: ICE, M = 6

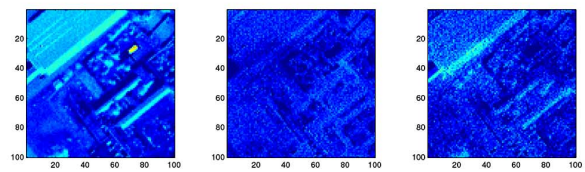

(g) 3: ICE, M = 6 (h) 3: ICE, M = 6 (i) 3: ICE, M = 6

Fig. 11. Proportion maps from the VCA runs with $\mathrm{M} = 3$ (a)–(c) and ICE, $\mathrm{M} = 6$ (d)–(i). This pair of result had the maximum EMD value. Thus, these set of results were the most distinct according to the EMD.

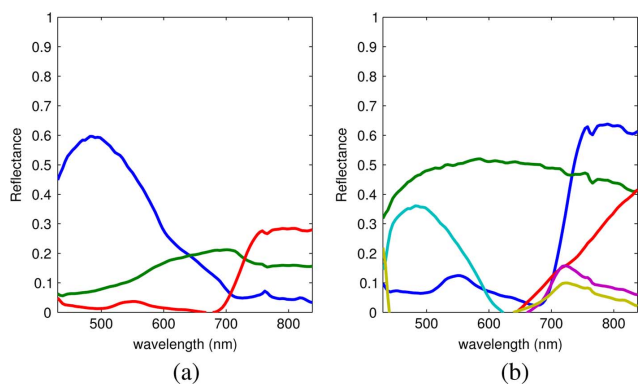

Fig. 12. Endmember spectra from the VCA with $\mathrm{M} = 3$ and ICE with $\mathrm{M} = 6$. This pair of result had the maximum EMD value in this experiment. (a) VCA, $\mathrm{M} = 3$—Blue: Water, Green: Building & Sidewalk, Red: Vegetation, (b) SPICE $\Gamma = 10$.

to compare the similarity in unmixing results on a per-pixel basis. However, it may be desireable or required to have one soft-matching identified for all pixels in a hyperspectral image. This can be accomplished by aggregating all proportion vectors and, then, compute the EMD once between the endmember sets and the aggregated proportion vectors. Thus, in this way, a single soft matching is determined for all pixels in the scene. For example, the aggregated proportion vectors could be the sum of the proportion vectors across all input pixels, i.e., $\mathbf{p}_{agg} = \sum_{n=1}^{N_x} \mathbf{p}_i$ and $\mathbf{q}_{agg} = \sum_{n=1}^{N_x} \mathbf{q}_i$. Then, the $\mathrm{EMD}_{tot,agg}$ would

be found by computing the EMD once with the aggregated proportion vectors. To illustrate the possible results, the Pavia experiment was repeated with this aggregated approach. The resulting pairwise EMD values are shown in Table IV. As can be seen, these results are extremely similar to those in Table III. In fact, nearly all $\max$, $\min$, and median values are found with the same pairwise results. This is a result of the fact that the overwhelming majority of pixels in an image will have a very consistent soft-matching between the endmember sets. However, as described in the following section, significant future work in the development of aggregated EMD approaches is needed. Namely, investigation into approach aggregation operators for the proportion values are needed and, as the behavior of the pointwise EMD has been examined here and in the previous EMD literature, the behavior of this aggregated EMD needs investigation.

V. Summary and Future Work

The EMD is shown herein to be an effective and flexible method for evaluating and comparing hyperspectral endmember estimation and spectral unmixing results. The EMD is a foundation on which one can compare results while incorporating both endmember and proportion values simultaneously. The method is also capable of comparing results with different numbers of endmembers. As shown in the experimental results, the EMD can effectively compare estimated endmembers and proportions to groundtruth values. The method is also able to compare and group sets of spectral unmixing results across various parameter settings for an unmixing algorithm or across different spectral unmixing algorithms.

Future work includes investigating additional methods of aggregating the point-wise EMD values for computation of $\mathrm{EMD}_{\mathrm{tot}}$. Currently, (10) is computed for each data point in a hyperspectral data set and, then, the sum is used to aggregate all of these values for a total EMD. Investigations can be conducted for considering different aggregation methods to additional comparison behaviors that can be used to group spectral unmixing results. Also, investigation into appropriate ground distances to be used within the proposed method for various applications will be conducted. For example, the use of set-based distances for a ground distance to account for spectral variability in endmember values and address the use of endmember bundles will be investigated. Finally, future work on the development of Aggregated EMD approaches is needed. Investigation into the methods for aggregating proportion values such that a single soft-matching is obtained is needed. Also, comparison of Aggregated EMD approaches and point-wise approaches is needed.

References

[1] G. Okin, D. Roberts, B. Murray, and W. Okin, "Practical limits on hyperspectral vegetation discrimination in arid and semiarid environments," *Remote Sens. Environ.*, vol. 77, no. 2, pp. 212–225, 2000.

[2] P. Dennison and D. Roberts, "The effects of vegetation phenology on endmember selection and species mapping in southern california chaparral," *Remote Sens. Environ.*, vol. 87, no. 2-3, pp. 123–135, 2003.

[3] O. Sonnetag, J. Chen, D. Roberts, J. Talbot, K. Halligan, and A. Govind, "Mapping tree and shrub leaf area indices in an ombrotrophic peatland through multiple endmember spectral unmixing," *Remote Sens. Environ.*, vol. 109, pp. 342–360, 2007.

[4] T. Rashed, J. Weeks, D. Robers, J. Rogan, and R. Powell, "Measuring the physical composition of urban morphology using multiple endmember spectral mixture models," *Photogramm. Eng. Remote Sens.*, vol. 69, no. 9, pp. 1011–1020, 2003.

[5] R. Powell, D. Roberts, P. Dennison, and L. Hess, "Subpixel mapping of urban land cover using multiple endmember spectral mixture analysis: Manaus, Brazil," *Remote Sens. Environ.*, vol. 106, pp. 253–267, 2007.

[6] L. Li and J. Mustard, "Highland contamination in lunar mare soils: Improved mapping with multiple endmember spectral mixture analysis," *J. Geophys. Res.*, vol. 108, 2003.

[7] J. Johnson, M. Staid, T. Titus, and K. Becker, "Shocked plagioclase signatures in thermal emission spectrometer data of mars," *Icarus*, vol. 180, pp. 60–74, 2006.

[8] J. Bioucas-Dias, A. Plaza, N. Dobigeon, M. Parente, Q. Du, P. Gader, and J. Chanussot, "Hyperspectral unmixing overview: Geometrical, statistical, and sparse regression-based approaches," *IEEE J. Sel. Topics Appl. Earth Observ. Remote Sens.*, vol. 5, no. 2, pp. 354–379, 2012.

[9] C. Hecker, M. van der Meijde, H. van der Werff, and F. van der Meer, "Assessing the influence of reference spectra on synthetic sam classification results," *IEEE Trans. Geosci. Remote Sens.*, vol. 46, no. 12, pp. 4162–4172, 2008.

[10] G. Martin and A. Plaza, "Region-based spatial preprocessing for endmember extraction and spectral unmixing," *IEEE Geosci. Remote Sens. Lett.*, vol. 8, no. 4, pp. 745–749, 2011.

[11] Z. Rabah, I. Farah, G. Mercier, and B. Solaiman, "A new method to change illumination effect reduction based on spectral angle constraint for hyperspectral image unmixing," *IEEE Geosci. Remote Sens. Lett.*, vol. 8, no. 6, pp. 1110–1114, 2011.

[12] Y. Rubner, C. Tomasi, and L. Guibas, "The earth movers distance as a metric for image retrieval," *Int. J. Comp. Vis.*, vol. 40, 2000.

[13] D. Anderson and A. Zare, "Spectral unmixing cluster validity index for multiple sets of endmembers," *IEEE J. Sel. Topics Appl. Earth Observ. Remote Sens.*, vol. 5, no. 4, pp. 1281–1295, 2012.

[14] D. Anderson, A. Zare, and S. Price, "Comparing fuzzy, probabilistic and possibilistic partitions using the earth mover's distance," *IEEE Trans. Fuzzy Sys.*, vol. 21, no. 4, pp. 766–775, 2012.

[15] D. Anderson, J. Bezdek, M. Popescu, and J. Keller, "Comparing fuzzy, probabilistic, and possibilistic partitions," *IEEE Trans. Fuzzy Sys.*, vol. 18, no. 5, pp. 906–918, 2010.

[16] N. Keshava and J. Mustard, "Spectral unmixing," *IEEE Sig. Proc. Mag.*, vol. 19, pp. 44–57, 2002.

[17] N. Keshava, "Distance metrics and band selection in hyperspectral processing with applications to material identification and spectral libraries," *IEEE Trans. Geosci. Remote Sens.*, vol. 42, no. 7, pp. 1552–1565, 2004.

[18] C.-I. Chang, "Spectral information divergence for hyperspectral image analysis," in *Proc. IEEE Geosci. RemoteSens. Symp.*, 1999, vol. 1, pp. 509–511, vol.1.

[19] H. Kuhn, *Naval Research Logistics Quarterly*, vol. 2, pp. 83–97, 1955.

[20] R. Sandler and M. Lindenbaum, "Nonnegative matrix factorization with earth mover's distance metric for image analysis," *IEEE Trans. Pattern Anal. Mach. Intell.*, vol. 33, no. 8, pp. 1590–1602, 2011.

[21] Q. Zhao, Z. Yang, and H. Tao, "Differential earth mover's distance with its applications to visual tracking," *IEEE Trans. Pattern Anal. Mach. Intell.*, vol. 32, no. 2, pp. 274–287, 2010.

[22] D. Xu, S. Yan, S. Lin, T. Huang, and S.-F. Chang, "Enhancing bilinear subspace learning by element rearrangement," *IEEE Trans. Pattern Anal. Mach. Intell.*, vol. 31, no. 10, pp. 1913–1920, 2009.

[23] M. Uddenfeldt, K. Hoashi, K. Matsumoto, and F. Sugaya, "Adaptive video news story tracking based on earth mover's distance," in *Proc. IEEE Int. Conf. Multimedia Expo*, 2006, pp. 1029–1032.

[24] H. Ling and K. Okada, "An efficient earth mover's distance algorithm for robust histogram comparison," *IEEE Trans. Pattern Anal. Mach. Intell.*, vol. 29, no. 5, pp. 840–853, 2007.

[25] D. Xu, S. Yan, and J. Luo, "Face recognition using spatially constrained earth mover's distance," *IEEE Trans. Image Process.*, vol. 17, no. 11, pp. 2256–2260, 2008.

[26] M. Bazaraa, J. Jarvis, and H. Sherali, *Linear Programming and Network Flows*. New York, NY, USA: Wiley, 2010.

[27] Y. Rubner, Code for the Earth Movers Distance (EMD) [Online]. Available: http://ai.stanford.edu/rubner/emd/default.htm
[28] S. Shirdhonkar and D. Jacobs, "Approximate earth movers distance in linear time," in *Proc. IEEE Conf. Computer Vision Pattern Recognit.*, 2008.
[29] A. M. Baldridge, S. J. Hook, C. I. Grove, and G. Rivera, "The aster spectral library version 2.0," *Remote Sens. Environ.*, vol. 9, 2008.
[30] M. Berman, H. Kiiveri, R. Lagerstrom, A. Ernst, R. Donne, and J. F. Huntington, "ICE: A statistical approach to identifying endmembers in hyperspectral images," *IEEE Trans. Geosci. Remote Sens.*, vol. 42, pp. 2085–2095, 2004.
[31] B. Somers, G. P. Asner, L. Tits, and P. Coppin, "Endmember variability in spectral mixture analysis: A review," *Remote Sens. Environ.*, vol. 115, no. 7, pp. 1603–1616, 2011.
[32] C. A. Bateson, G. P. Asner, and C. A. Wessman, "Endmember bundles: A new approach to incorporating endmember variability into spectral mixture analysis," *IEEE Trans. Geosci. Remote Sens.*, vol. 38, no. 2, pp. 1083–1093, 2000.
[33] A. Zare and P. Gader, "Pce: Piece-wise convex endmember detection," *IEEE Trans. Geosci. Remote Sens.*, vol. 48, no. 6, pp. 2620–2632, 2010.
[34] A. Zare, P. Gader, and G. Casella, "Sampling piecewise convex unmixing and endmember extraction," *IEEE Trans. Geosci. Remote Sens.*, 2013.
[35] O. Eches, N. Dobigeon, C. Mailhes, and J.-Y. Tourneret, "Bayesian estimation of linear mixtures using the normal compositional model: Application to hyperspectral imagery," *IEEE Trans. Image Process.*, vol. 19, no. 6, pp. 1403–1413, 2010.
[36] S. Holzwarth, A. Muller, M. Habermeyer, R. Richter, A. Hausold, S. Thiemann, and P. Strobl, "Hysens-dais 7915/rosis imaging spectrometers at dlr," in *Proc. 3rd EARSeL Workshop on Imaging Spectroscopy*, 2003.
[37] J. M. P. Nascimento and J. M. Bioucas-Dias, "Vertex component analysis: A fast algorithm to unmix hyperspectral data," *IEEE Trans. Geosci. Remote Sens.*, vol. 43, no. 4, pp. 898–910, 2005.
[38] A. Zare and P. Gader, "Sparsity promoting iterated constrained endmember detection for hyperspectral imagery," *IEEE Geosci. Remote Sens. Lett.*, vol. 4, no. 3, pp. 446–450, Jul. 2007.
[39] T. C. Havens, J. C. Bezdek, and J. M. Keller, "A new implementation of the co-vat algorithm for visual assessment of clusters in rectangular relational data," in *Proc. Int. Conf. Artif. Intell. Soft Comput.: Part I*, 2010, pp. 363–371.
[40] T. Havens and J. Bezdek, "An efficient formulation of the improved visual assessment of tendency (ivat) algorithm," *IEEE Trans. Knowledge Data Eng.*, vol. 24, no. 5, pp. 813–822, 2012.
[41] T. Havens, J. Bezdek, J. Keller, and M. Popescu, "Clustering in ordered dissimilarity data," *Int. J. Intell. Syst.*, vol. 24, no. 5, pp. 504–528, 2009.

Alina Zare received the Ph.D. degree in computer and information science and engineering (ECE) in 2008 from the University of Florida, Gainesville, FL, USA.

She is currently an Assistant Professor in ECE at the University of Missouri, MO, USA. Her research interests include machine learning, computational intelligence, pattern recognition, Bayesian methods, SONAR analysis, target detection, and hyperspectral image analysis.

Derek T. Anderson received the Ph.D.degree in electrical and computer engineering (ECE) in 2010 from the University of Missouri, Columbia, MO, USA.

He is currently an Assistant Professor in ECE at Mississippi State University, MS, USA. His research interests include fusion, pattern recognition, clustering, computer vision, linguistic summarization of human activity from video and hyperspectral image analysis.